Wearable Loop Sensor for Unambiguous and High-Resolution Joint Kinematics Monitoring

Vigyanshu Mishra, *Member, IEEE*, and Asimina Kiourti, *Senior Member, IEEE*

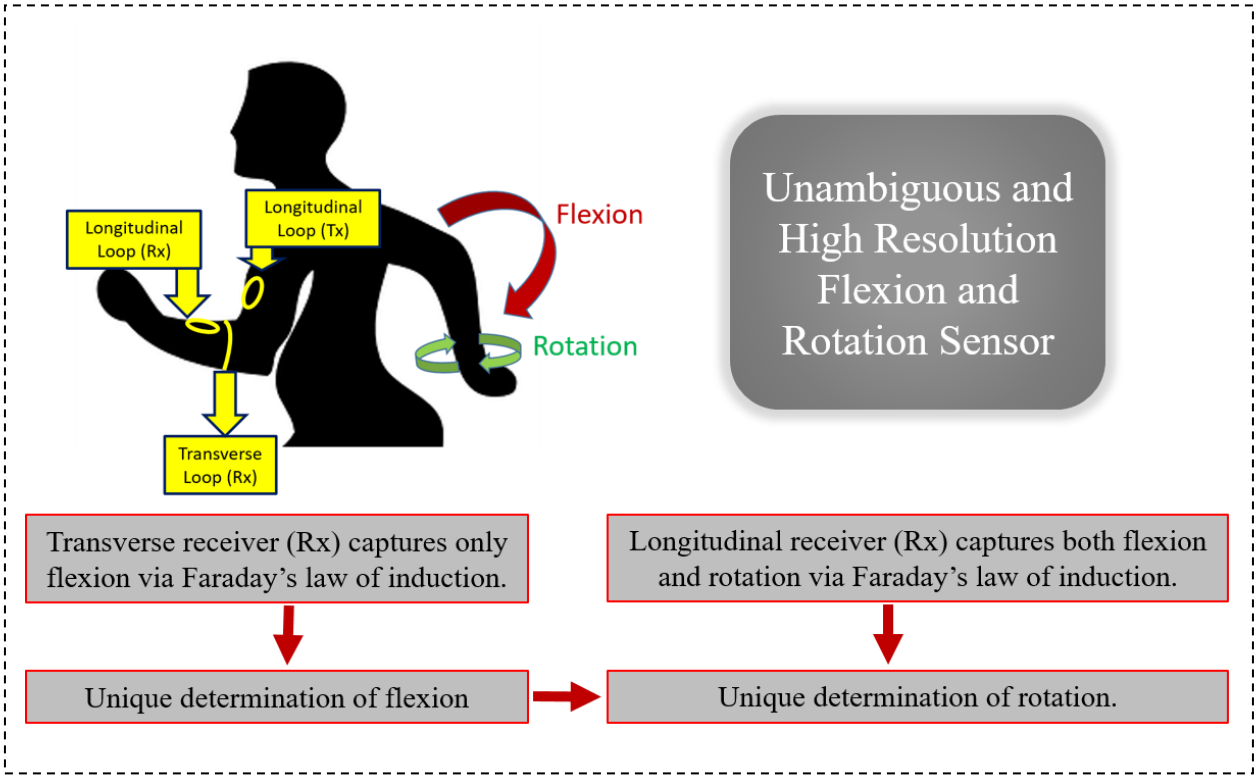

Proposed wearable loop sensor and corresponding operating principle.

Take-Home Messages

- A new wearable sensor is proposed that relies on combinations of longitudinal and transverse loops to monitor joint kinematics in real-world settings that are, unavoidably, subject to noise, at unprecedented resolution.
- The sensor is demonstrated to capture joint flexion and rotation unambiguously and at clinically relevant resolution, while overcoming limitations in state-of-the-art wearable kinematics sensors.
- The sensor is relevant in the detection, prevention, and rehabilitation of diverse motor disabling conditions, such as Parkinson's, Traumatic Brain Injury, and Anterior Cruciate Ligament injuries, among others.
- Compared to the closest competing technology, we report an improvement in angular resolution by up to 153.8 times under low noise and 38.4 times under high noise.
- The sensor's high resolution also empowers the monitoring of fine movements that could not be previously captured outside the lab.

Wearable Loop Sensor for Unambiguous and High-Resolution Joint Kinematics Monitoring

Vigyanshu Mishra, *Member, IEEE*, and Asimina Kiourti, *Senior Member, IEEE*

Abstract We have recently introduced wearable loop sensors that are based on Faraday's law to seamlessly monitor real-world kinematics while overcoming shortcomings in the state-of-the-art. The latest sensor of this wearable ecosystem employs loops in longitudinal configuration (LC) to monitor joint flexion and rotation, but its resolution degrades due to ambiguities (more than one states of motion for the same sensor reading). Here, we demonstrate that resolution degradation exacerbates in the presence of noise, and report a new wearable sensor that eliminates ambiguities to improve resolution. The sensor entails a longitudinal-transmitter placed above the joint and a transverse-receiver, followed by a longitudinal-receiver, placed below the joint (namely, longitudinal-transverse-longitudinal configuration, LTLC). These two receivers help segregate flexion and rotation, thereby eliminating ambiguities in deciphering angles and boosting resolution manifolds as compared to LC. Proof-of-concept simulation and *in vitro* experimental results show excellent agreement. Compared to LC, flexion angle resolution improves by up to 153.8 times (0.013° to 2°) under low noise and 38.4 times (0.13° to 5°) under high noise. Improvement for rotation angles is similar/higher. Specific absorption rate results also confirm excellent electromagnetic safety. LTLC is the first in the wearable loop ecosystem that can monitor both joint flexion/rotation without ambiguities, improving resolution even in the presence of noise. LTLC shows high promise for monitoring clinically relevant kinematics in real-world settings that are, unavoidably, subject to noise. Its high resolution also empowers the monitoring of fine movements that could not be previously captured outside the lab.

***Keywords* — Flexion, longitudinal loops, monitoring, resolution, rotation, transverse loops, wearables.**

I. Introduction

MONITORING human body kinematics ushers a plethora of benefits in healthcare (detection, prevention and rehabilitation), sports (training, prevention, and rehabilitation), human-machine interfaces (gesture recognition, virtual reality, and gaming), animation movies, and biomedical research [1]. A wearable technology that can monitor movements seamlessly and without impeding the individual's natural movement, in real-time, accurately, and reliably could provide a strong impetus to the development in these areas [1].

Recently, we introduced the first ecosystem of wearable loop sensors [2]–[4] that are based on Faraday's law of induction to seamlessly and precisely monitor joint kinematics outside the lab (unlike camera-based systems [5], [6]); reliably over time (unlike inertial measurement units, IMUs [7]–[9]); without requiring line-of-sight (unlike time-of-flight sensors [8], [10]); and without obstructing natural motion (unlike bending sensor [11]–[13]). Referring to Table I, our transverse configuration (TC) sensor [2] employs two loops – one above and one below the joint – wrapped around the limb. It can only monitor flexion (i.e., its operation is insensitive to rotation) and exhibits an angular resolution that varies from 0.02° to 0.9° for an example 0° to 100° range of flexion. The longitudinal configuration (LC) sensor [3] in Table I employs three loops – one above and two below the joint – with their plane parallel to the limb axis. It enables both flexion and rotation monitoring, but suffers from inherent ambiguities. That is, the same sensor reading corresponds to multiple combinations of flexion/rotation angles. These ambiguities are resolved via post-processing, but end up degrading resolution. Our previous work [3] indicated a fixed 2° resolution for an example 0° to 100° range of flexion. However, this resolution degrades significantly in the presence of high noise conditions, as will be demonstrated in this paper and summarized in Table I,

TABLE I
Wearable Loop Ecosystem for Monitoring Joint Kinematics

		TC	LC	LTLC (Proposed)
Advantages over State-of-the-Art Motion Capture	**Works outside the lab**	Yes (+)	Yes (+)	Yes (+)
	Seamless	Yes (+)	Yes (+)	Yes (+)
	Insensitive to line-of-sight	Yes (+)	Yes (+)	Yes (+)
	Allows natural motion	Yes (+)	Yes (+)	Yes (+)
	Reliable vs. time	Yes (+)	Yes (+)	Yes (+)
Monitors Joint Flexion		Yes (+)	Yes (+)	Yes (+)
Monitors Joint Rotation		No (-)	Yes (+)	Yes (+)
Unambiguous* detection of flexion (θ_f) and rotation (θ_r) angles		-	No (-)	Yes (+)
Resolution under low noise for flexion range 0° to 100°		0.02°-0.9°	2° fixed (same for rotation)	0.013°-0.37° (similar/better for rotation)
Resolution under high noise for flexion range 0° to 100°		0.2°-10°	5° fixed (same for rotation)	0.13°-5° (similar /better for rotation)

*Ability to detect (θ_f, θ_r) uniquely, i.e., no two states (θ_f, θ_r) correspond to

Manuscript received January 28, 2022. This work was supported by the National Science Foundation under Grants 1842531 and 2042644.

V. Mishra and A. Kiourti are with the ElectroScience Laboratory, Department of Electrical and Computer Engineering, The Ohio State University, Columbus, OH, 43212, USA (e-mails: mishra.186@osu.edu, kiourti.1@osu.edu).

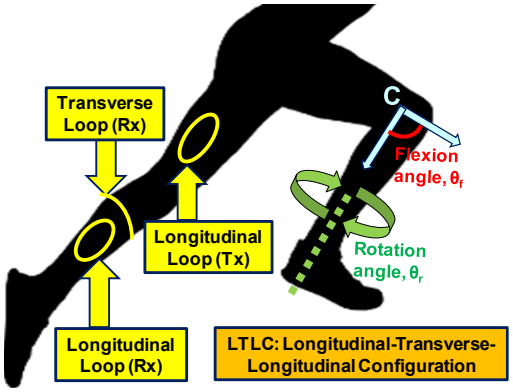

Fig. 1. Proposed LTLC sensor for unambiguous monitoring of joint flexion/rotation by uniquely capturing θ_f through transverse Rx and consequently θ_r via longitudinal Rx.

making the sensor inadequate for a vast range of clinical applications.

In this work, we take a major step forward and propose a new sensor that: (a) maintains the benefits of the wearable loop ecosystem outlined in the first five rows of Table I, (b) monitors both flexion and rotation without any ambiguities, in turn, improving resolution in the presence of noise, (c) empowers/inspires monitoring of more sophisticated joints in the future, and (d) evaluates, quantifies, and compares resolution of all three loop sensors (TC, LC, and LTLC) for the first time. The novel idea is a design that segregates flexion and rotation. We refer to this sensor as longitudinal-transverse-longitudinal configuration, LTLC, and herewith study its performance numerically and upon tissue-emulating phantoms. Per Table I, flexion angle resolution improves by up to 153.8 times (0.013° to 2°) under low noise and up to 38.4 times (0.13° to 5°) under high noise. Improvement for rotation angles is similar or higher. LTLC can also be reconfigured to monitor flexion only (a feature that is not possible with LC), improving the TC resolution by up to 2.4 times under low noise and 2.5 times under high noise.

The rest of the paper is organized as follows. Section II discusses the sensor's operating principle. Section III reports proof-of-concept numerical and experimental methods, and results. Section IV provides a detailed quantitative comparison amongst LTLC, TC, and LC. Section V explains why only a particular combination of longitudinal and transverse loops provides a feasible solution and discusses loop placement for reliable operation and Specific Absorption Rate (SAR). The paper concludes in Section VII.

II. Operating Principle

As shown in Fig. 1, the proposed LTLC sensor consists of three loops: one longitudinal loop that is placed above the joint and acts as transmitter (Tx), one transverse loop that is placed below the joint and acts as receiver (Rx), and one longitudinal loop that is placed below the joint and below the aforementioned Rx to again act as Rx. These loops are all electrically small resonant loops (ESRLs) (more details in Section III). They operate at radio frequency and support only time-varying current, without any space variation, due to their electrically small dimension. Note that sensor operation is not restricted to the knee joint as depicted in Fig. 1 and can be used for other joints with similar biomechanics (e.g., elbow joint). Tx and Rx loops are placed within the near-field region and are inductively coupled to each other via Faraday's law of induction, such that:

$$V_{Rx,t} = -\frac{d}{dt}\iint \boldsymbol{B_{Tx,lt}} \cdot \widehat{\boldsymbol{n_{Rx,t}}}\, ds, \quad (1)$$

$$V_{Rx,l} = -\frac{d}{dt}\iint \boldsymbol{B_{Tx,ll}} \cdot \widehat{\boldsymbol{n_{Rx,l}}}\, ds, \quad (2)$$

where, $V_{Rx,t}$ and $V_{Rx,l}$ represent the voltage induced on the transverse Rx and longitudinal Rx respectively; $\boldsymbol{B_{Tx,lt}}$ and $\boldsymbol{B_{Tx,ll}}$ are the magnetic flux density vectors produced by the time-varying current flowing in the longitudinal Tx at the location of the transverse and longitudinal Rx loops respectively; and $\widehat{\boldsymbol{n_{Rx,t}}}$ and $\widehat{\boldsymbol{n_{Rx,l}}}$ represent the normal surface area vectors for the transverse and longitudinal Rx, respectively.

With change in flexion angle (θ_f in Fig. 1), the transmission coefficient (a measure of voltage) for both receiving loops changes. This is attributed to changes in $\widehat{\boldsymbol{n_{Rx,t}}}$ and $\widehat{\boldsymbol{n_{Rx,l}}}$ (i.e., changes of the loops' angular orientation in space) as well as changes in $\boldsymbol{B_{Tx,lt}}$ and $\boldsymbol{B_{Tx,ll}}$ (due to changes in the distance/location of the each of the Rx with respect to the Tx). However, with a change in rotation angle (θ_r in Fig. 1), neither $\widehat{\boldsymbol{n_{Rx,t}}}$ nor $\boldsymbol{B_{Tx,lt}}$ change for the transverse Rx due to spatial symmetry. By contrast, for the longitudinal Rx, both $\widehat{\boldsymbol{n_{Rx,l}}}$ and $\boldsymbol{B_{Tx,ll}}$ change with change in θ_r. Thus, both receiving loops can capture θ_f independent of each other, whereas the longitudinal Rx can also capture θ_r.

The ability of the longitudinal Rx to monitor both θ_f and θ_r gives rise to ambiguities (see definition in Section I). This is the same limitation we encountered with the LC sensor in the past [3]. Here though, the presence of the transverse Rx readily resolves any ambiguity by uniquely determining θ_f while being insensitive to rotation. Once θ_f is uniquely determined, the longitudinal Rx can be used to uniquely identify θ_r. In summary, LTLC segregates θ_f and θ_r information on the transverse and longitudinal Rx, respectively, to uniquely determine the correct state of motion (θ_f, θ_r).

Note that the property of the transverse Rx of being insensitive to rotation is similar to TC [2]. However, unlike TC, LTLC has a longitudinal Tx and hence the symmetry property can be utilized only when the two Rx are placed on the part of the limb that performs rotation (i.e., on the shank and not on the thigh in the case of a knee joint sensor). It is also interesting to note that LTLC can be configured either as flexion/rotation sensor (data collected from both receiving loops) or as flexion-only sensor (data collected from only the the transverse Rx). This reconfigurability was not possible with any of the previous designs of Table I.

III. Methods and Results

A. Numerical and In Vitro Experimental Methods

As shown in Fig. 2, the cylindrical 3.9-cm-radius limb model employed in [2], [3] is used for numerical simulations.

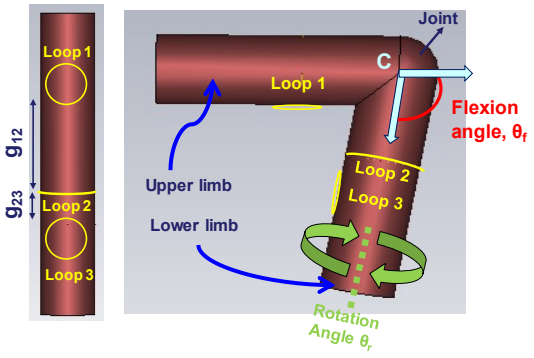

Fig. 2. Simulation set-up for LTLC using electrically small resonant loops (ESRLs) on a canonical limb model. Set-up is same as in Fig.1, where Loop 1 (longitudinal) acts as transmitter, while Loop 2 (transverse) and Loop 3 (longitudinal) act as receivers.

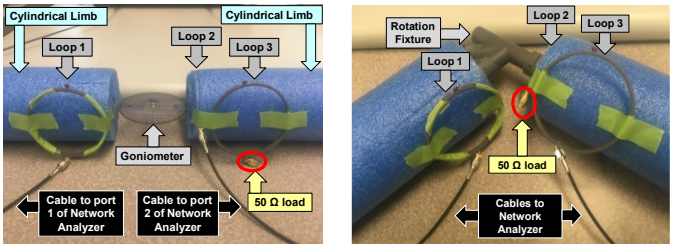

(a) (b)

Fig. 3. Experimental setups for: (a) flexion measurements using goniometer, and (b) rotation measurements using 3D printed fixture.

Similar to Fig. 1, loop 1 represents the longitudinal Tx, loop 2 represents the transverse Rx, and loop 3 represents the longitudinal Rx. They are placed upon the limb with a gap of g_{12}=10 cm between loops 1 and 2 (choice of g_{12} will become clear in Section V), and g_{23}=1 cm between loops 2 and 3 (a small and practical number is arbitrarily selected as shown in the past to improve power reception and rotation angular resolution [3]). Transverse and longitudinal loops are designed and placed in the same way as for TC in [2] and LC in [3], respectively. Specifically, they have a radius of 4 cm, are made of 0.254-mm-diameter copper wire, and placed at a spacing of 0.1 cm from the limb. Similar to [2], [3] a capacitor is added in series to make each loop resonant at 32 MHz. This resonant operating frequency and corresponding loop size (circumference ~ 0.02λ) makes the loops electrically small. In other words, they are electrically small resonant loops (ESRLs) where the "electrically small" part enables robust performance despite changes in tissue dielectric properties, while the "resonant" part ensures better power reception [2], [3]. This allows usage of Styrofoam to emulate limbs in experiments as discussed later. The abovementioned configuration is utilized throughout this work, except, the spacing of longitudinal loops from the limb is increased by 0.15 cm for experimental validation as will become clear next. Simulations are performed for θ_f and θ_r varying from 0° to 90° and 0° to 50°, respectively, at a step size of 10° using the frequency domain solver of CST Microwave Studio® [14]. Rotation simulations are performed at two indicative values of θ_f, viz. 0° and 80°. Subsequently, transmission between loops 1 and 2, and between loops 1 and 3, are obtained, represented by the corresponding

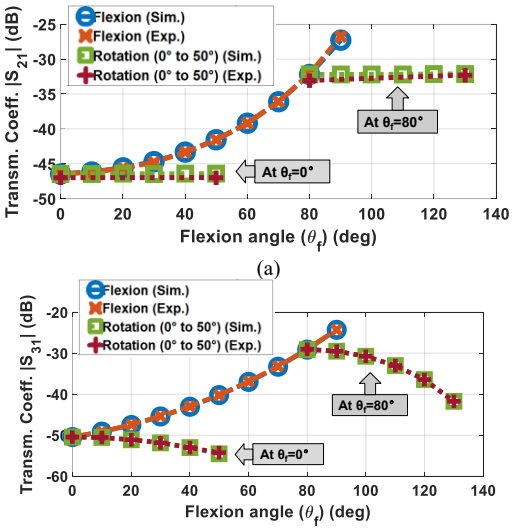

Fig. 4. Superimposed numerical simulation and experimental results: (a) $|S_{21}|$ showing feasibility of monitoring joint flexion while being insensitive to rotation, and (b) $|S_{31}|$ showing feasibility of monitoring both flexion and rotation.

transmission coefficient magnitudes, $|S_{21}|$ and $|S_{31}|$, respectively.

As shown in Fig. 3, the experimental setup employs Styrofoam limbs with motion capabilities enabled by a goniometer for flexion and a 3D-printed fixture for rotation [2], [3]. Transverse and longitudinal loops are fabricated and incorporated on the limbs. Specifically, the transverse loop is directly wrapped around the limb, while the longitudinal loop is adhered to a 3D printed circular fixture to maintain shape and size [3] (explaining the 0.15 cm increase in spacing from the limbs). All flexion measurements are again performed for θ_f varying from 0° to 90° at a step size of 10° for both $|S_{21}|$ and $|S_{31}|$. Rotation measurements for $|S_{21}|$ are carried out at θ_r = 0° and 50°, as deemed sufficient to validate unaltered value across the range. For $|S_{31}|$, rotation measurements are carried out for θ_r varying from 0° to 50° at a step size of 10°. Same as in numerical simulations, all rotation measurements are performed at two indicative values of θ_f, viz. 0° and 80°. $|S_{21}|$ and $|S_{31}|$ are measured in succession, one at a time, using a two-port network analyzer (PNA-L N5235A). The third loop that is not connected to the network analyzer is connected to a 50 Ω load to emulate a realistic scenario [3] [see Fig. 3].

Note that this setup is for proof-of-concept demonstration and can be tweaked per application needs following guidelines discussed in the past for TC [2] and LC [3]. For instance, change in limb size can be accommodated via change in radius of TC, and requirement of range of motion via gap between Tx and Rx loops.

B. Results

Simulation and experimental results at 32 MHz are superimposed and summarized in Fig. 4. Flexion and rotation curves are integrated in the same plot [3]. As expected, $|S_{21}|$ captures changes in θ_f uniquely by being insensitive to rotation, while $|S_{31}|$ captures both flexion and rotation. This leads to segregation of information, i.e., θ_f is uniquely tied to $|S_{21}|$, while θ_r is uniquely tied to $|S_{31}|$. In other words, $|S_{21}|$

can, by itself, monitor joint flexion and, when combined with $|S_{31}|$, one can determine the state of motion (θ_f, θ_r) without ambiguities. Improvement in the resulting performance as compared to TC and LC is quantified in Section IV. Flexion information present in $|S_{31}|$ is also available, if required (for instance, to improve noise performance). In addition, there is excellent agreement between simulation and experiments for both flexion and rotation, thereby validating the results. A slight shift in $|S_{21}|$ values for the rotation curve can be attributed to g_{12} being slightly larger than 10 cm. This happens because the rotation fixture has a length of 10 cm between the Styrofoam edges, and the transverse loop (loop 2) cannot be placed on the edge of the Styrofoam. Also, any minor rotation on the transmitting loop side of the limb can also cause slight change in values; this would not happen in an *in vivo* experiment where the thigh (or equivalent part of the body) does not rotate.

IV. Performance Comparison with TC and LC

A. Methodology

As discussed in Section II, the proposed LTLC sensor can be configured either as flexion-only sensor (similar to TC) or as flexion/rotation sensor (similar to LC). Here, the performance of LTLC is compared vs. TC for flexion and vs. LC for flexion/rotation. Loop design parameters, as described for the numerical setup in Section III.A, are kept the same for TC [2] and LC [3] to enable fair comparison across all three designs. To quantify performance, we derive an approximation of angular resolution for each design under different levels of noise. This is the first time that our wearable loop ecosystem of Table I is studied in the presence of different levels of noise and across the range of motion.

To approximate angular resolution, one can use the transmission coefficient dynamic range, i.e., difference between maximum and minimum value of the transmission coefficient across the range of motion [2], [3]. This approximation is valid as the higher the dynamic range, the smaller the changes in flexion/rotation angle that can be determined for any given sensitivity of the measuring instrument. Notably, the approximation becomes more accurate if one considers the dynamic range for a smaller range of flexion/rotation angles. Referring to Fig. 4, this is because a better linear approximation can be made on such smaller intervals of a non-linear curve. We use this strategy to obtain an approximate angular resolution for TC and LTLC wherein 10° steps are used and a linear fit is assumed in between. For LC, dynamic range does not directly translate into angular resolution, due to presence of ambiguities. However, the post-processing algorithm of LC also utilizes a similar 10° step-size and linear fit to determine angular resolution for an unambiguous detection in [3], thereby enabling an equivalent comparison across all three designs.

Here, it is worth acknowledging that the aforementioned step-size and linear fit assumption will naturally introduce a small error. Hence, the angular resolution obtained is hereafter termed as 'approximate' angular resolution. For instance, across all three designs (TC, LC, and LTLC) the maximum error in estimating data points via linear approximation is 0.5 dB across the flexion range, the minimum error is 0.01 dB, while errors are <0.12 dB for $\theta_f <$ 80°, i.e. error reduces significantly with reducing flexion angles due to decreasing non-linearity [see Fig. 4]. Similar behavior is expected from rotation curves. Note that the step size of 10° can be reduced to further improve the accuracy of translation from dynamic range to angular resolution: ideally, the best translation would be obtained for an infinitesimally small step-size. However, this requires infinite number of data points that, in turn, entail infinite number of numerical simulations. Given this tradeoff, a suitably small step-size is chosen with sufficiently small error which does not require too many data points and at the same time provides a good practical estimate.

In the subsequent analysis, two noise scenarios are considered: low and high. The measuring instrument that records transmission coefficient values would typically have several digits of precision. However, under the impact of different levels of noise, the digit of precision would vary. In an ideal scenario, all digits of precision provide consistent readings for any number of measurements made. However, as the level of noise starts to increase, the digit farthest to the decimal point would start to fluctuate. As the influence of noise increases, fluctuation would propagate towards digits closer to the decimal point, thereby introducing measurement unreliability for the fluctuating digit. Thus, naturally, the reliable digits (digits that remain consistent across multiple measurements for the same set-up) after the decimal point would decrease as the level of noise increases. Here, we assume that, under low noise, two digits of precision can be measured. This would degrade to one digit under high noise conditions. Note that this determines both the transmission coefficient value and minimum difference between two closest values that can be recorded from the instrument.

The aforementioned definition of low vs. high noise provides a quite practical representation for two relative noise scenarios that helps compare the three designs. If the definition were to change in terms of digits of precision, the absolute numbers obtained would change, but the relative comparison would still remain valid. The latter is the focus of this section.

Based on the above, the approximate angular resolution can be calculated in a three-step process. First, selecting the noise condition sets the smallest value that can be measured via the measuring instrument. Second, dividing the dynamic range for each 10° step size by the above smallest value will yield the total number of steps in which each 10° interval can be further subdivided. And, third, by dividing the 10° value with the obtained number of steps, one can get the approximate angular resolution for each 10° interval.

B. Results

Angular resolution results obtained for flexion and rotation are summarized in Fig. 5. As seen, resolution is fixed for LC across all flexion/rotation angles, but improves significantly with increasing angles for TC and LTLC. The reason is that the presence of ambiguities in LC ties it to a fixed resolution, even though the dynamic range improves

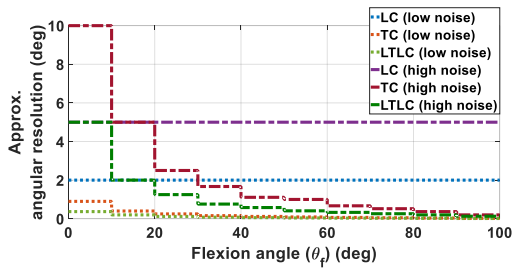

(a)

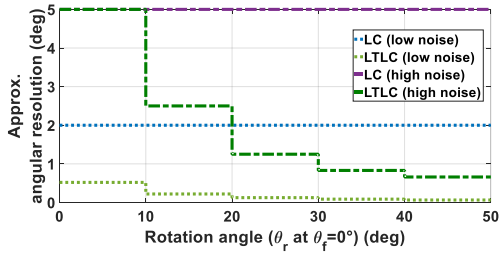

(b)

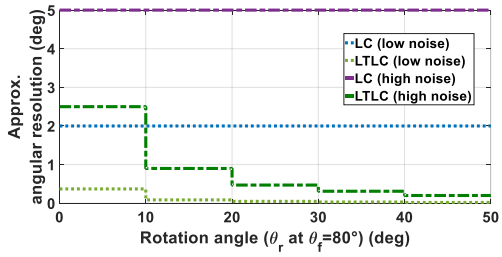

(c)

Fig. 5. Comparison of approximate angular resolution of (a) TC, LC and LTLC during flexion, (b) LC and LTLC during rotation (at $\theta_f = 0°$), and (c) LC and LTLC during rotation (at $\theta_f = 80°$) under low and high noise conditions.

with increasing angles [3]. By contrast, for TC and LTLC, the dynamic range directly translates to angular resolution. Hence, the angular resolution consistently improves with increasing flexion/rotation angles as the dynamic range (or slope of flexion/rotation curve) increases [see Fig. 5 and 4] and hence the need to define range of resolution values.

Specifically, under low noise conditions, flexion resolution for LC is fixed at 2° across the range of motion. For LTLC, it ranges from 0.37° to 0.013° [see Fig. 5(a)], thereby providing an improvement of 5.4 to 153.8 times. TC depicts similar behavior to LTLC, but shows 1.5 to 2.4 times degraded resolution as compared to LTLC [see Fig. 5(a)].

Under high noise conditions, and as expected, performance degrades for all designs. Flexion resolution for TC varies from 10° to 0.2°, for LC it becomes 5°, and for LTLC it varies from 5° to 0.13° across the range of motion [see Fig. 5(a)]. Again, the behavior of LTLC and TC is similar (i.e., improved resolution with increasing flexion angle) with LTLC outperforming TC by 1.5 to 2.5 times across the range. Compared to LC, performance improvement of up to 38.4 times (5° to 0.13°) is observed.

Similar results are obtained for rotation at θ_f=0° [see Fig. 5(b)]. Particularly, under low and high noise, LC again provides 2° and 5° fixed resolutions, respectively. LTLC exhibits resolution varying from 0.52° (3.8 times improvement) to 0.064° (31.2 times improvement) under low noise, and from 5° (no improvement) to 0.66° (7.5 times

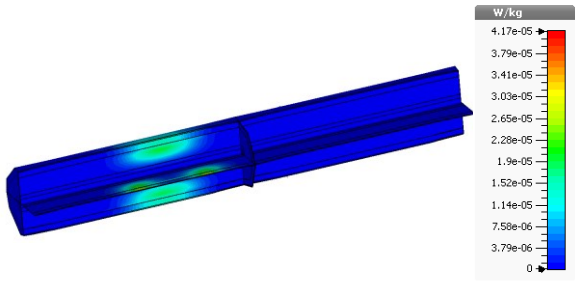

Fig. 6. Distribution of specific absorption rate averaged over 1g of tissue (SAR_{1g}) across multiple cross-sections

improvement) under high noise. As expected, performance of LTLC improves considerably for rotation at $\theta_f = 80°$ due to higher dynamic range [see Fig. 4(b) and 5(c)]. Particularly, performance improves from 5.4 times to 100 times under low noise, and from 2 to 25 times under high noise.

C. *Discussion*

For both flexion and rotation, resolution degrades under noisy conditions as expected, and LTLC demonstrates better noise performance as compared to both TC and LC. It is also worth noting that change in performance from low to high noise is the highest for TC, followed by LTLC, and least for LC, especially at lower flexion angles. That is, the impact of noise is highest for TC, followed by LTLC and then LC at lower angles [see Fig. 5]. This happens because of the high dynamic range of LC [3] that, unfortunately, cannot be fully translated to angular resolution due to ambiguities. To get a quantitative perspective, TC, LTLC, and LC exhibit dynamic range of 14.24 dB, 25.83 dB, and 33.03 dB respectively for θ_f 0° to 100°, and 1.37 dB, 2.82 dB, and 7.25 dB respectively for θ_f 0° to 40°. Hence, LTLC significantly outperforms LC under both low and high noise conditions by eliminating ambiguities and allowing complete utilization of the dynamic range. LTLC also outperforms TC because of the improved dynamic range or slope of the flexion curve that directly translates to resolution.

Thus, LTLC combines the advantages of both TC (unambiguous flexion monitoring) and LC (improved dynamic range and feasibility of monitoring both flexion and rotation). Concurrently, LTLC eliminates disadvantages of both TC (low dynamic range and inability to monitor rotation) and LC (presence of ambiguities that degrade resolution despite the high dynamic range). Finally, given the above features of LTLC, it outperforms both TC and LC under noisy conditions.

V. Additional Considerations

A. *Specific Absorption Rate (SAR) Studies*

Specific absorption rate averaged over 1g of tissue (SAR_{1g}) is evaluated with the setup of Fig. 2, yet with a multilayered limb model consisting of skin, fat, muscle, cortical bone and bone marrow to obtain a realistic estimate [2], [3]. Distribution of SAR_{1g} obtained for an input power of 1 mW (prescribed as maximum reference power by IEEE 802.15.6 [15]) at 32 MHz is shown in Fig. 6 for multiple cross-sections. Maximum SAR_{1g} of 41.7 µW/Kg is obtained which is well below the prescribed value of 1.6 W/Kg by Federal Communications Commission (FCC) [16]. In fact, to

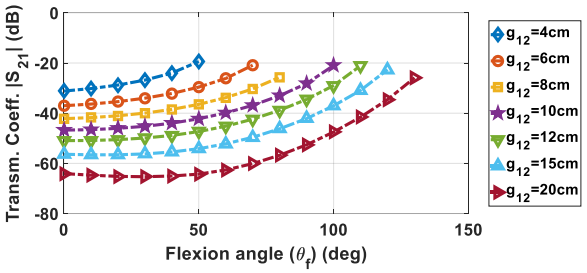

Fig. 7. Importance of g_{12} selection for desired range of motion, resolution and reliable operation displayed via $|S_{21}|$ for different values of g_{12}.

hit the maximum SAR_{1g} of 1.6 W/Kg set by FCC, an input power level of 38.3 W is required which is way beyond the practical implementation for any wearable technology.

B. Gap (g_{12}) Selection

Gap (g_{12} in Fig. 2) between loops 1 and 2 is one of the most crucial design aspects for reliable operation. To demonstrate this, the setup of Fig. 2 is used with g_{12} varying from 4 to 12 cm in steps of 2 cm, along with g_{12} equal to 15 and 20 cm. Transmission coefficient results obtained are shown in Fig. 7. For g_{12} > 10 cm, slight ambiguity starts to arise in the flexion angle, i.e. the same $|S_{21}|$ values corresponds to two different flexion angles for lower values of θ_f (i.e., the curve goes down and then back up). This behavior increases further and moves to higher angles as g_{12} keeps increasing (for instance, this trend is more visible on the plot for g_{12}=20 cm). However, for $g_{12} \leq 10$ cm there is no such ambiguity and LTLC can be used to monitor both flexion and rotation reliably. It must be noted that this value of g_{12} is valid for the setup employed in this work and may vary depending on the shape and size of the anatomical geometry. Hence, g_{12} needs to be selected carefully during the design process. Additionally, as expected, the range of motion reduces and resolution improves as g_{12} is reduced similar to TC [2], and LC [3].

C. Other Combinations of Transverse and Longitudinal loops

The idea of using both transverse and longitudinal loops to segregate flexion and rotation has been made clear. However, there exist four different combinations of transverse and longitudinal loops to create a three-loop configuration. Using a transverse loop as Tx allows for two configurations, i.e., TTLC (transverse-transverse-longitudinal configuration), and TLTC (transverse-longitudinal- transverse configuration). Using a longitudinal loop as Tx allows for two additional configurations, i.e., LTLC (this work), and (d) LLTC (longitudinal-longitudinal-transverse configuration). Here, we explain why only LTLC provides the intended performance.

TTLC can monitor flexion but with degraded resolution, similar to TC [2]. It is also not suitable for rotation monitoring because: (a) the transverse Rx is insensitive to rotation, and (b) the longitudinal Rx with transverse Tx would yield results similar (not same due to slight asymmetry) to Fig. 4(a) which again show insensitivity to rotation. Here, even if the locations of Tx and Rx are switched to break the spatial symmetry, still rotation either cannot be monitored (at $\theta_f = 0°$ because of symmetry) or can be monitored with very poor resolution at lower flexion angles. Furthermore, both TLTC and LLTC cannot be used because of strong asymmetry introduced by the longitudinal Rx (loop 2) in between loops 1 and 3. This causes strong ambiguity in flexion monitoring itself, wherein the same transmission coefficient value corresponds to two different flexion angles, as shown for LLTC in Fig. 8. Hence, only LTLC is one such special configuration that provides the desired combination of transverse and longitudinal loops.

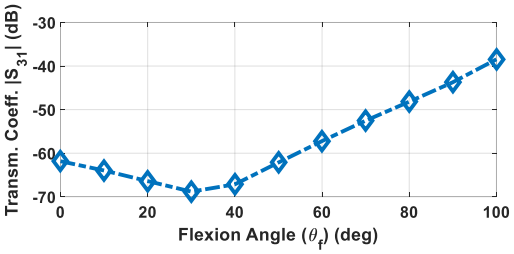

Fig. 8. Ambiguity in flexion measurement for longitudinal-longitudinal-transverse configuration (LLTC) rendering it unsuitable for flexion monitoring.

VI. Conclusion

We introduced a new three-loop sensor design, namely longitudinal-transverse-longitudinal-configuration (LTLC) that can monitor joint flexion or/and rotation unambiguously. The sensor was shown to outperform both previously reported TC and LC sensors along with preserving their benefits over the state-of-the-art. *In vitro* experimental results showed excellent congruence with numerical simulations, confirming practical feasibility. A detailed quantitative comparison among TC, LC, and LTLC demonstrated the superiority of the proposed design (due to higher dynamic range and lack of ambiguities as compared to TC and LC, respectively). For instance, when compared to TC, an improvement in resolution by up to 2.4 (low noise) and 2.5 (high noise) times was obtained across flexion angles. Under low noise conditions, LTLC showed improvement by 5.4 times (0.37° to 2°) to 153.8 times (0.013° to 2°) as compared to LC for flexion, and 3.8 times (0.52° to 2°) to 31.2 times (0.064° to 2°) for rotation at zero flexion angle. Under high noise conditions, LTLC showed an equivalent (both 5°) to 38.4 times (0.13° to 5°) improvement for flexion and similar performance for rotation. Rotational resolution was found to improve considerably at higher flexion angles under both low and high noise conditions. Furthermore, uniqueness of LTLC was highlighted as opposed to other combinations of transverse and longitudinal loops. Gap selection and its importance was discussed for reliable operation, and SAR studies confirmed electromagnetic safety for human use.

In the future, we will integrate the design on garments via conductive e-threads, introduce wireless functionality for cable free operation, and validate the design through *in vivo* dynamic experiments on human subject participants. Once fully developed, the sensor can be employed for monitoring

clinically relevant joint kinematics for prevention, detection, rehabilitation and understanding of motor disabling conditions in healthcare, such as Parkinson's, Traumatic Brain Injury, and Anterior Cruciate Ligament injuries, among others.

REFERENCES

[1] V. Mishra and A. Kiourti, "Wearable Sensors for Motion Capture," in *Antenna and Sensor Technologies in Modern Medical Applications*, John Wiley & Sons, Ltd, 2021, pp. 43–90.

[2] V. Mishra and A. Kiourti, "Wrap-Around Wearable Coils for Seamless Monitoring of Joint Flexion," *IEEE Trans. Biomed. Eng.*, vol. 66, no. 10, pp. 2753–2760, Oct. 2019.

[3] V. Mishra and A. Kiourti, "Wearable Electrically Small Loop Antennas for Monitoring Joint Flexion and Rotation," *IEEE Trans. Antennas Propag.*, vol. 68, no. 1, pp. 134–141, Jan. 2020.

[4] V. Mishra, N. R. Kieves, S. C. Jones, and A. Kiourti, "In Vivo Monitoring of Dog's Knee Flexion Using Wearable Wrap-Around Coils," in *2020 IEEE International Symposium on Antennas and Propagation and North American Radio Science Meeting*, Jul. 2020, pp. 229–230.

[5] V. B. Zordan and N. C. Van Der Horst, "Mapping optical motion capture data to skeletal motion using a physical model," in *Proceedings of the 2003 ACM SIGGRAPH/Eurographics symposium on Computer animation*, Goslar, DEU, Jul. 2003, pp. 245–250.

[6] E. E. Stone and M. Skubic, "Unobtrusive, Continuous, In-Home Gait Measurement Using the Microsoft Kinect," *IEEE Trans. Biomed. Eng.*, vol. 60, no. 10, pp. 2925–2932, Oct. 2013.

[7] M. El-Gohary and J. McNames, "Shoulder and Elbow Joint Angle Tracking With Inertial Sensors," *IEEE Trans. Biomed. Eng.*, vol. 59, no. 9, pp. 2635–2641, Sep. 2012.

[8] C. Einsmann, M. Quirk, B. Muzal, B. Venkatramani, T. Martin, and M. Jones, "Modeling a wearable full-body motion capture system," in *Ninth IEEE International Symposium on Wearable Computers (ISWC'05)*, Oct. 2005, pp. 144–151.

[9] S. C. Mukhopadhyay, "Wearable Sensors for Human Activity Monitoring: A Review," *IEEE Sens. J.*, vol. 15, no. 3, pp. 1321–1330, Mar. 2015.

[10] Y. Qi, C. B. Soh, E. Gunawan, K.-S. Low, and A. Maskooki, "A Novel Approach to Joint Flexion/Extension Angles Measurement Based on Wearable UWB Radios," *IEEE J. Biomed. Health Inform.*, vol. 18, no. 1, pp. 300–308, Jan. 2014.

[11] J. H. M. Bergmann, S. Anastasova-Ivanova, I. Spulber, V. Gulati, P. Georgiou, and A. McGregor, "An Attachable Clothing Sensor System for Measuring Knee Joint Angles," *IEEE Sens. J.*, vol. 13, no. 10, pp. 4090–4097, Oct. 2013.

[12] P. Gibbs and H. H. Asada, "Wearable conductive fiber sensor arrays for measuring multi-axis joint motion," in *The 26th Annual International Conference of the IEEE Engineering in Medicine and Biology Society*, Sep. 2004, vol. 2, pp. 4755–4758.

[13] C. Li *et al.*, "Flexible CNT-array double helices Strain Sensor with high stretchability for Motion Capture," *Sci. Rep.*, vol. 5, no. 1, pp. 1–8, Nov. 2015.

[14] "Electromagnetic Simulation Solvers | CST Studio Suite." Accessed: Apr. 8, 2022. [Online]. Available: https://www.3ds.com/products-services/simulia/products/cst-studio-suite/solvers/.

[15] S. Movassaghi, M. Abolhasan, J. Lipman, D. Smith, and A. Jamalipour, "Wireless Body Area Networks: A Survey," *IEEE Commun. Surv. Tutor.*, vol. 16, no. 3, pp. 1658–1686, Third 2014.

[16] FCC OET, "Evaluating compliance with FCC guidelines for human exposure to radio frequency electromagnetic fields," Bulletin 65, Washington, DC. Available: https://www.fcc.gov/general/oet-bulletins-line. [Accessed: 8-Apr-2022].

Asimina Kiourti (S'10, M'14, SM'19) received the Diploma degree in electrical and computer engineering from the University of Patras, Patras, Greece, in 2008, the M.Sc. degree in technologies for broadband communications from University College London, London, U.K., in 2009, and the Ph.D. degree in electrical and computer engineering from the National Technical University of Athens, Athens, Greece, in 2013.

She is currently an Assistant Professor of Electrical and Computer Engineering at The Ohio State University and the ElectroScience Laboratory, Columbus, OH, USA. From 2013 to 2016, she served as a Post-Doctoral Researcher and then a Senior Research Associate at the ElectroScience Laboratory. During her career, she has co-authored 1 book, 12 book chapters, 5 granted patents, over 65 journal papers, and over 110 conference papers/abstracts. Her research interests include bio-electromagnetics, wearable and implantable antennas, sensors for body area applications, and functionalized e-textiles.

Dr. Kiourti has received several scholarly awards, including the 2022 Early Career Distinguished Scholar Award by The Ohio State University, the 2021 NSF CAREER award, the 2021 40 Under 40 recognition by Columbus Business First, the 2018 URSI Young Scientist Award, the 2014 IEEE Engineering in Medicine and Biology Society (EMB-S) Young Investigator Award, the 2012 IEEE Microwave Theory and Techniques Society (MTT-S) Graduate Fellowship for Medical Applications, and the 2011 IEEE Antennas and Propagation Society (AP-S) Doctoral Research Award.

She is currently serving as the Senior Editor of the IEEE Open Journal of Antennas and Propagation, the Editor of the Bioelectromagnetics column of the IEEE Antennas and Propagation Magazine, and an Associate Editor for the IEEE Transactions on Antennas and Propagation, the IEEE Journal of Electromagnetics, RF and Microwaves in Medicine and Biology, and the IEEE Antennas and Propagation Magazine.